Performance assessment of discrete wavelet transform for de-noising of FBG sensors signals embedded in asphalt pavement

Performance Assessment of Discrete Wavelet Transform for De-noising of FBG Sensors Signals Embedded in Asphalt Pavement

Ali Golmohammadi [*1], Navid Hasheminejad [2], David Hernando [2], Steve Vanlanduit [3], Wim Van den bergh [2]

*corresponding author

[1] seyedali.golmohammaditavalaei@uantwerpen.be, SuPAR Research Group, Faculty of Applied Engineering, University of Antwerp, Antwerp, Belgium

[2] SuPAR Research Group, Faculty of Applied Engineering, University of Antwerp, Antwerp, Belgium

[3] InViLab Research Group, Faculty of Applied Engineering, University of Antwerp, Antwerp, Belgium

ABSTRACT

In recent years, the Fiber Bragg Grating (FBG) sensor technology has been increasingly utilized as an optical measurement system in various engineering applications, particularly for structural health monitoring (SHM) purposes. This trend can be attributed to the inherent benefits of FBG sensors, such as their small size, immunity to electromagnetic interference, resistance to corrosion, and high accuracy and sensitivity. Various factors cause noise in the FBG sensor signal, which has a significant effect on measurement precision. As a result, de-noising plays an important role in the use of FBG sensor systems. In this study, strain data collected from FBG sensors embedded in a road section were used to evaluate the performance of discretized wavelet transform (DWT) for denoising FBG signals. The presence of noise poses a significant challenge in accurately measuring low-amplitude strains and light loads. To address this issue, various approaches have been investigated, including the selection of appropriate mother wavelets, levels of decomposition, thresholding functions, and thresholding selection approaches, with the aim of identifying the optimal parameters for effective denoising. The results show that FBG signals could be denoised successfully and low amplitude strains appeared completely without any loss of valuable data.

Keywords: FBG sensor, signal de-nosing, optical measurement, discretized wavelet transform, asphalt pavement

1. INTRODUCTION

The ongoing advancement of optical technology has led to fiber Bragg grating (FBG) sensors with excellent immunity to electromagnetic interference, corrosion resistance, high sensitivity, and a tiny body. FBG sensors are widely applied in civil, aerospace, and other fields due to their relatively low cost and unmatched advantages over conventional sensors. However, in engineering applications, various factors create noise in the collected FBG signal, which has a significant impact on precision[1].

Optical return loss (ORL) is a phenomenon in which light reflected back from an optical fiber or component causes interference with the transmitted light. In FBG sensors, ORL can cause noise in the reflected signal, leading to errors in the measurement of strain, temperature, or other physical parameters [2]. Several factors, including imperfections in the fiber or FBG fabrication, mismatched connectors, patch cords, mechanical splices, and environmental factors such as temperature changes or vibrations, can cause ORL in FBG sensors. To reduce the impact of ORL, advanced signal processing algorithms can filter out the ORL-induced noise and improve the precision of the measurement.

In order to improve the quality of FBG signals, some studies on denoising were conducted [3], but they had some limitations. The previous studies used the fast Fourier transform (FFT) and moving average filter to deal with the noise of FBG signals [4], but the coarse scale of the Fourier transform hindered noise removal. As the discrete wavelet transform (DWT) provides enhanced time-frequency localization and multi-rate filtering, it can be utilized to reduce noise in signals. Using DWT-based denoising, a signal is decomposed into a number of sub-bands with various frequency ranges. The DWT coefficients of the signal components are high and constrained to a single frequency band whereas the coefficients of the noise components are low and dispersed throughout the various frequency bands [5]. Therefore, denoising can be achieved by suppressing the small coefficients. The success of DWT-based denoising depends on parameters such as the mother wavelet utilized, the number of decomposition levels (DLs), the threshold function employed, and the type of thresholding approach performed [6]. The best mother wavelets are Daubechies, Symlets, Coiflets, and Bio-orthogonal because they produce excellent reconstruction results [7,8]. Furthermore, it is important to choose an optimal number of DLs so that the levels are adequately distributed across the useful and unwanted signal components.

The most popular thresholding approaches for DWT-based signal denoising are rigsure, sqtwolog, heursure, and minimaxi. The threshold function, which is the last decision factor, controls how the wavelet coefficients are handled when the approximative threshold value is employed. The two types of thresholding functions utilized for signal denoising are hard thresholding (HT) and soft thresholding (ST), each with benefits and drawbacks. Therefore, choosing the appropriate parameters for denoising is a significant difficulty for scholars working on signal data [9].

In this section, some previous studies on the denoising of FBG signals have been reviewed. For example, Chen et al. [10] developed a new FBG wavelength demodulation approach that uses an improved

denoising technique based on translational invariant wavelet and a Gaussian fitting peak finding methodology. They used the enhanced translational invariant wavelet without the threshold adjust factor to improve the de-noising of the FBG sensor output. This denoising approach is intended to be combined with the Gaussian fitting peak finding algorithm to provide a high wavelength demodulation accuracy of the signal. The outcomes of the simulation demonstrated that a far better degree of precision can be achieved with a small wavelength measurement error that is less than 1 pm. According to Zhang et al. [11], there are several undesirable noise sources between the local circuits and the remote sensing fiber that are difficult to remove and that reduce the system's performance. They used two FBG sensors with different central wavelengths to create two interferometric signals as a unique technique to decrease the noise caused along the transmission fiber. A theoretical study revealed that most of the noise could be removed by subtracting the two signals, and simulation calculations demonstrated that the remaining noise is less than 1% under usual conditions. Besides, an analysis was performed on the variables that influenced the amount of residual noise. In another investigation, a new wavelet adaptive threshold technique developed by Chen et al. [12] was utilized to filter a noisy spectrum signal from an FBG system. A threshold function was used to improve the noisy FBG signal after the best wavelet basis and decomposition layer were selected through simulation. In another study, Jiang et al. [13] presented a denoising algorithm that combined local complementary ensemble empirical mode decomposition (LCEEMD) and lifting wavelet transform technology (LWT) to address crosstalk noise in high-capacity fiber grating multiplexing networks. The proposed method utilizes complementary ensemble empirical mode decomposition (CEEMD) to decompose the original spectral signal and the normalization permutation entropy (NPE) to identify high-frequency nonlinear sequences in low-order intrinsic mode function for suppressing random noise. The high-frequency intrinsic mode function is further decomposed using LWT, which enhanced filtering accuracy. Also, Su et al. [14] discussed using Phase-sensitive optical time-domain reflectometer (Φ-OTDR) for long-distance measurements and applied fast non-local means (NLM) filtering, increasing noise suppression ratio (NSR) by 10 dB, peak signal-to-noise ratio (PSNR) by 12 dB, and SSIM from 0.9361 to 0.9931. The study also explored parameter effects. Besides, Wu et al. [15] proposed an improved denoising algorithm with wavelet theory and a hybrid approach with a bandpass filter. Furthermore, Lv et al. [16] proposed a precise multi-peak detection algorithm using wavelet packet denoising and Hilbert transform that outperformed other methods in noise reduction and achieved high stability and accuracy in real-time temperature detection, making it suitable for FBG monitoring in noisy conditions with faster computation.

In this work, information collected from FBG sensors embedded in a road section for pavement monitoring was utilized to assess the efficiency of the discretize wavelet transform (DWT) for de-noising FBG sensor signals. Various mother wavelets, levels of decomposition, thresholding functions, and thresholding selection approaches were tested to find the best de-noising parameters that successfully eliminate the noise that hides low amplitude strain measurements and light loads. Finally, the

performance of this method was compared with other signal filtering methods such as low-pass filter, median filter, and moving average filter. The results showed that FBG signals could be properly de-noised and low amplitude strains could be identified without losing any data.

2. RESEARCH METHODOLOGY

FBG signal denoising based on DWT requires three steps, as illustrated in Figure 1, including:

I. Decomposition of noisy FBG signals into selected-level of wavelet coefficients.
II. Applying a threshold using a thresholding function and a threshold selection rule to the coefficients.
III. Reconstruction of the denoised FBG signal using the remaining coefficients.

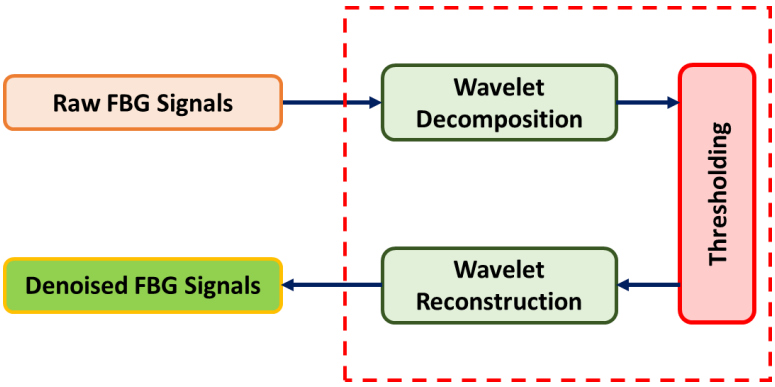

Figure 1 *Proposed denoising technique flow*

Raw strain data was collected during a pavement monitoring campaign conducted at the Port of Antwerp on May 17, 2022. The pavement section is composed of 21 cm of asphalt concrete (AC) and 40 cm of crushed stone. An FBG fiber with 12 sensing points was placed across the top of the crushed stone prior to laying the first asphalt lift. Thus, the FBG sensors capture the maximum horizontal strain in the transverse direction (i.e., perpendicular to the direction of traffic) at the bottom of the AC layer. The measurements were conducted with an 8-channel FBG-Scan 908 interrogator at a sampling frequency of 200 Hz; the data were collected and processed with ILLumiSense v2.3.5.5 and MATLAB software, respectively. Concurrent with the FBG measurements, the researchers annotated the timestamps and number of axles of all vehicles that drove over the instrumented section during the monitoring campaign. The workflow of the monitoring system is illustrated in Figure 2.

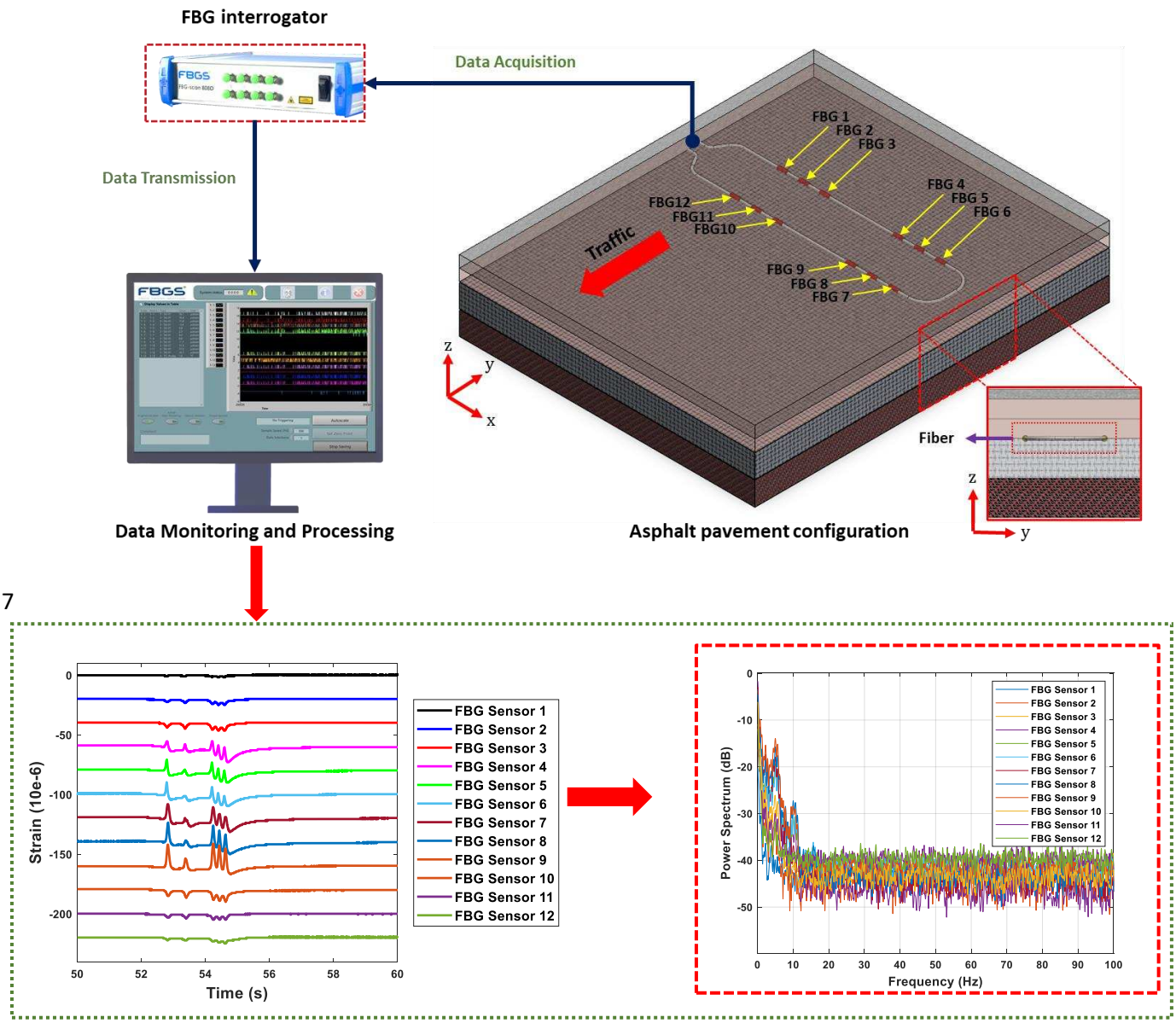

Figure 2 *Workflow of monitoring system*

As can be seen in Figure 2, all data were transformed from the time domain to the frequency domain using the Fourier transform to investigate the power spectrum of FBG signals in decibels (dB). The power spectrum refers to the distribution of power over the different frequencies that make up the signal. The shape of the power spectrum of an FBG signal depends on the characteristics of the FBG itself and the properties of the light that is reflected by the FBG. It is evident that there is a constant power spectrum between -40 and -50 dB for all frequencies higher than 10 Hz. Generally, a constant power spectrum value over a wide range of frequencies could indicate uniform background noise. In a noise-free signal, the power spectrum should exhibit peaks at specific frequencies that correspond to the signal's spectral content. However, in the presence of noise, the power spectrum can be contaminated by random

fluctuations that spread over a wide range of frequencies. Therefore, this noise should be removed using filtering methods to improve the FBG signals. Figure 3 (a) and (b) display the clean and noisy response signals, respectively, of FBG sensor 9 in response to a passing car (between the first set of dashed lines) and a 5-axle truck (between the second set of dashed lines). The original signal exhibits discretization noise that needs to be eliminated using an appropriate denoising method. The resulting clean signal can then serve as a ground truth for evaluating denoising performance (we will artificially add noise to the ground truth signals)

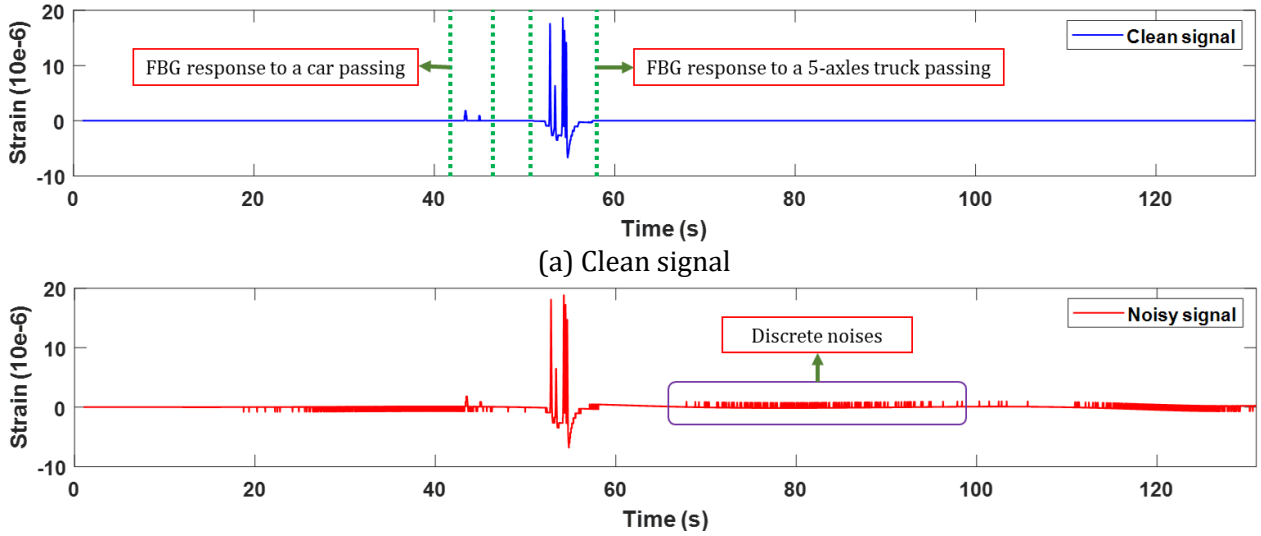

(a) Clean signal

(b) Nosy signal

Figure 3 *FBG sensor response to passing a car and 5-axle truck*

2.1. FBG SIGNAL DECOMPOSITIONS

The noisy FBG signal $x(n)$ was decomposed using DWT and the following selected mother wavelets: Daubechies, Symlets, Coiflet, and Biorthogonal. Using a high-pass filter (HPF) and a low-pass fitter (LPF) with impulse responses of $u(n)$ and $v(n)$, respectively, the noisy FBG signal $x(n)$ is decomposed into detailed (d) coefficients and approximation (a) coefficients. Then, both the approximate and the detailed coefficients are downsampled by a factor of two to obtain the next level coefficients. The following equation gives the wavelet filter bank structure required for L-level decomposition [17]:

$$x(n) = \sum_{j=1}^{L} d_j(n) + a_j(n) \tag{1}$$

Here, $d_j(n)$, and $a_j(n)$, $(j = 1, 2, \ldots, L)$ are the j-level detailed and approximation coefficients that denote the reconstructed sub-band signals. During decomposition, the signal-to-noise ratio (SNR) value is used to determine the ideal number of decomposition levels (DL).

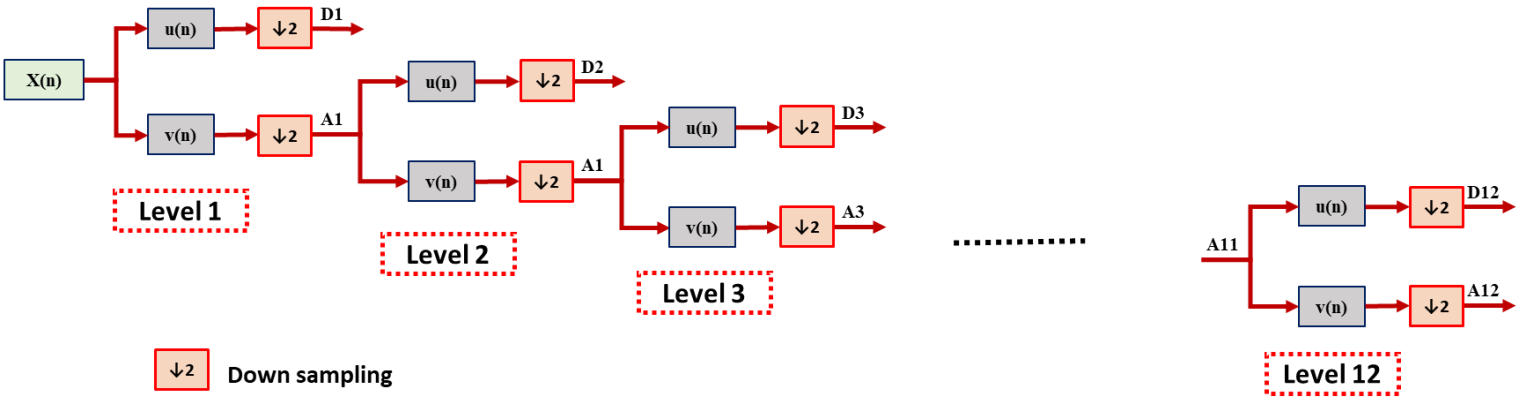

Figure 4 *FBG signal decomposition using DWT*

The noisy FBG signal is decimated into separate frequency bands by gradually filtering with HPF and LPF throughout the wavelet decomposition process, as shown in Figure 4. Using Nyquist's rule, half of the samples are eliminated after filtering. The signal is consequently down sampled by a factor of two, eliminating half of the total samples. The following equations represent one-level decomposition [18] :

$$\tilde{x}_{high}(k) = \sum_{n} x(n) \circledast u(2k - n) \tag{2}$$

$$\tilde{x}_{low}(k) = \sum_{n} x(n) \circledast v(2k - n) \tag{3}$$

where $\tilde{x}_{high}(k)$ and $\tilde{x}_{low}(k)$ are the outputs of the HPF and LPF, respectively, after a two down sampling (reducing high-frequency signal components with a digital lowpass filter). The convolution operation is denoted by the symbol $\circledast$ in Equations (2) and (3). The outputs of the HPF and LPF are the detailed coefficients and approximation coefficients, respectively. In this study, the noisy FBG signal was decomposed into several levels, and the optimal level of decomposition is discussed in further sections. As an example, a 6-level decomposition of a noisy FBG signal can be observed in Figure 5. Note that a total of seven coefficients were obtained: one is the approximation coefficient (a_6) and six are details coefficients ($d_1, d_2, d_3, \dots, d_6$).

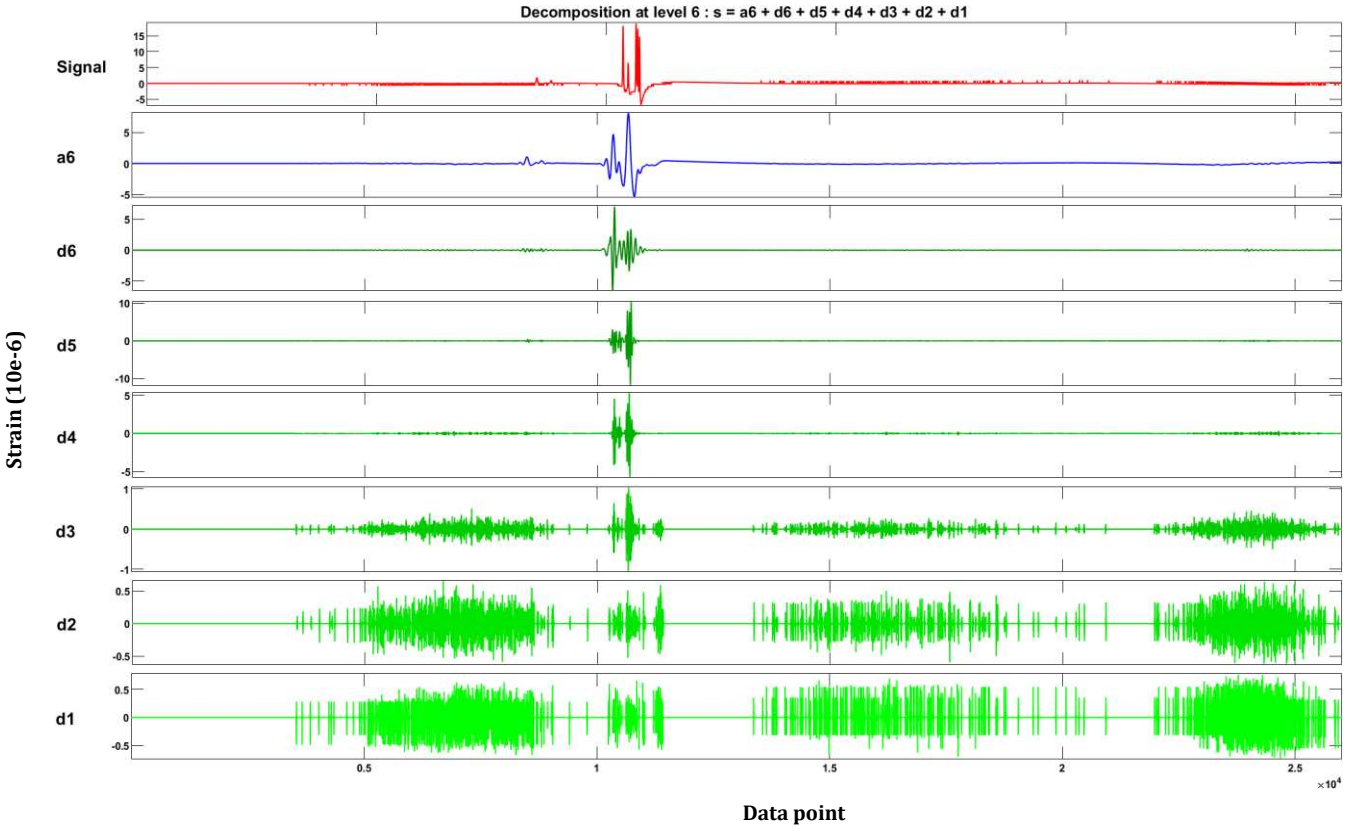

Figure 5 *Six-level decomposition of noisy FBG signal using DWT*

2.2. DETAILED COEFFICIENT THRESHOLDING AND RESCALING

The threshold value chosen for the technique is another important variable that has an impact on the effectiveness of denoising. If the chosen threshold value is set too high, some critical information in the signal may be filtered out, and if it is set too low, substantial noise may remain in the signal. The thresholding process that was used to convert the input FBG signal $x(n)$ into the estimated denoised FBG signal $\hat{X}(n)$ is represented by the following equation:

$$\hat{X}(n) = THR(x(n), \lambda) \tag{4}$$

Here, THR and λ represent the thresholding function and threshold value, respectively. In wavelet thresholding, the threshold value is used to modify the wavelet coefficients. The basic idea behind thresholding is to remove small wavelet coefficients while shrinking large wavelet coefficients. The obtained coefficients are then utilized for selective DWT inverse reconstruction. When comparing the two thresholding functions, hard thresholding (HT) is the more straightforward option because of simplicity, but it might result in discontinuities in the denoised signal. Soft thresholding (ST), on the other hand, has a smaller estimate error and produces better results. The following equation gives the definition of the HT function, which is seen in Figure 6(a)[19]:

$$\widehat{W} = \begin{cases} W & |W| \geq \lambda \\ 0 & |W| < \lambda \end{cases} \tag{5}$$

The ST function is illustrated in Figure 6(b) and determined by the equation below:

$$\widehat{W} = \begin{cases} sgn(W) \cdot (|W| - \lambda) & |W| \geq \lambda \\ 0 & |W| < \lambda \end{cases} \quad (6)$$

where λ is the threshold value and W denotes the wave coefficient.

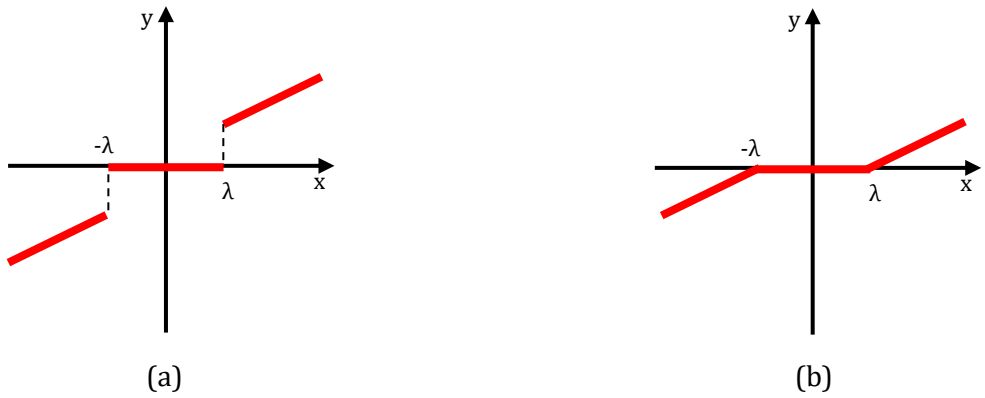

Figure 6 *Thresholding functions: (a) Hard Thresholding (HT) (b) Soft Thresholding (ST)*

2.3. THRESHOLDING TECHNIQUES

The thresholding techniques evaluated in this study were rigrsure, sqtwolog, heursure, and minimaxi. Thresholding selection criteria are composed of mathematical computations that may provide a realistic noise threshold.

2.3.1. Sqtwolog Criterion

This approach was suggested by Donoho and Johnstone. The threshold values are determined by applying the universal approach (square root record) expressed by [20,21]:

$$th_j = \sigma_j \sqrt{2 \log N_j} \quad (7)$$

where N_j is the length of the noisy signal and σ_j is median absolute deviation (MAD), which is defined as:

$$\sigma_j = \frac{MAD_j}{0.6745} \quad (8)$$

where MAD_j is the median of the absolute value of the j-level detail coefficients.

2.3.2. Rigrsure Criterion

An unbiased risk estimator is provided by the Rigrsure threshold selection rule given by [20,21]:

$$th_j = \sigma_j \sqrt{T_i} \quad (9)$$

where T_i is the i-th coefficient wavelet square (minimum risk coefficient) selected from the vector $T = [T_1, T_2, \dots, T_N]$ that contains the wavelet coefficient square values, ranging from small to large, and σ_j is the noisy signal's standard deviation.

2.3.3. Heursure Criterion

Combining Sqtwolog and Rigrsure techniques results in the Heursure threshold selection principle. The Sqtwolog approach provides superior threshold estimate when the SNR is very low, as opposed to the Rigrsure method [20,21].

2.3.4. Minimaxi Criterion

Minimaxi selection principle utilizes a fixed threshold to provide a minimax efficiency for the root mean square error against an ideal method, as follows [20,21]:

$$th_j = \begin{cases} \sigma(0.3936 + 0.10829 \log_2 N) & N > 32 \\ 0 & N < 32 \end{cases} \quad (10)$$

Here, $\sigma = median\left(\frac{|\omega|}{0.6745}\right)$ and ω is vector of wavelet coefficient at unit scale.

2.4. SIGNAL RECONSTRUCTION

The signal is reconstructed using its threshold coefficients, and this process is accomplished by an up-sampling operation. For this purpose, the higher-level detailed coefficients and approximation coefficients are up-sampled by a factor of 2 and fed through related HPF and LPF, respectively, to reconstruct the denoised FBG signal. These filters are referred to as reconstruction filters, which are orthogonal to the analytical filters employed in the decomposition process. The sum of the outputs from these two filters, as shown in Figure 7, produces approximation coefficients for the reconstruction of the next phases. Eventually, the Inverse Discrete Wavelet Transform (IDWT) on $\tilde{x}(n)$ FBG signal is then used to approximate the original FBG signal, as indicated in the following equation:

$$S(n) = IDWT\left(\tilde{x}(n)\right) \quad (11)$$

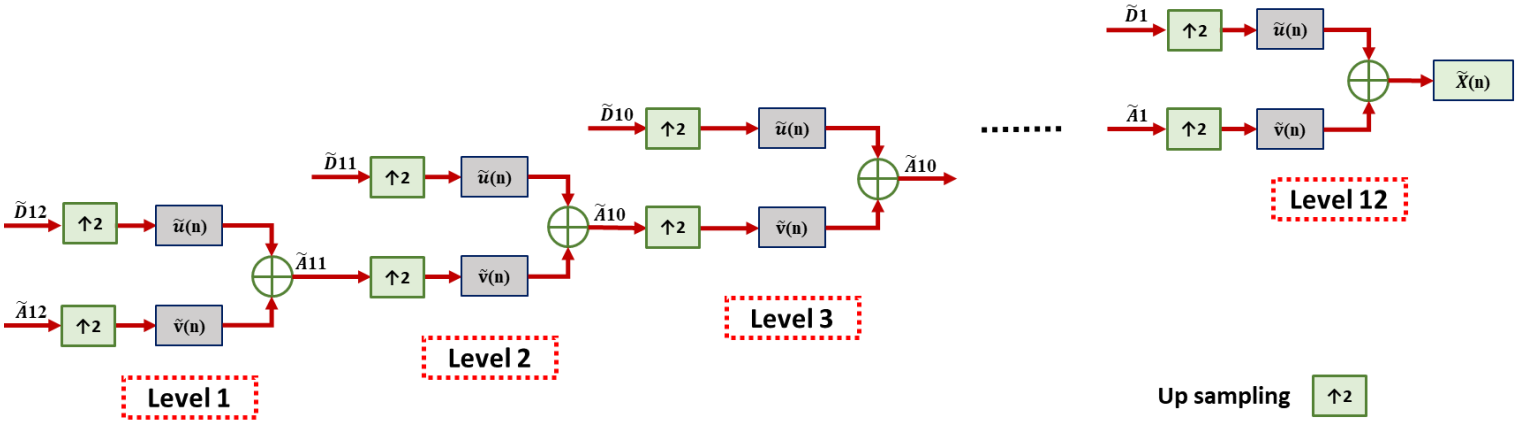

Figure 7 *FBG signal reconstruction using IDWT*

2.5. PERFORMANCE METRICS

The performance of the de-noising algorithms was evaluated in terms of the mean squared error (MSE), normalized mean squared error (NMSE), root mean squared error (RMSE), normalized root mean squared error (NRMSE), percentage poot mean square difference (PRD), and signal-to-noise-ratio (SNR). MSE calculates the deviation between the clean FBG signal and the denoised version of the FBG signal, and its formula is as follows:

$$MSE = \frac{1}{N}\sum_{n=1}^{N}(x(n) - \tilde{x}(n))^2 \quad (11)$$

The definition of the NMSE is [22]:

$$NMSE = \frac{\sum_{n=1}^{N}(x(n) - \tilde{x}(n))^2}{\sum_{n=1}^{N}(x(n))^2} \quad (12)$$

In order to make the error independent of the original signal, normalization is essential. The third metric, RMSE, is expressed in Equation (13) and is used to calculate the sample standard deviation of the differences between the denoised signal and the clean signal.

$$RMSE = \sqrt{\frac{1}{N}\sum_{n=1}^{N}(x(n) - \tilde{x}(n))^2} \quad (13)$$

Nevertheless, RMSE is insufficient to indicate the FBG signal quality. To overcome this limitation, the normalized form of the RMSE, known as the normalized RMSE (RMSE), was calculated:

$$NRMSE = \sqrt{\frac{\sum_{n=1}^{N}(x(n) - \tilde{x}(n))^2}{\sum_{n=1}^{N}(x(n))^2}} \quad (14)$$

Moreover, PRD is a distinctive distortion metric that is frequently utilized to assess how well denoising algorithms work and demonstrates the accuracy of reconstruction by a point-to-point correlation with the initial results. This metric is characterized by the following equation:

$$PRD = \sqrt{\frac{\sum_{n=1}^{N}(x(n) - \tilde{x}(n))^2}{\sum_{n=1}^{N}(x(n))^2}} \times 100 \quad (15)$$

The most critical parameter for determining the level of noise in the FBG signal is SNR and is defined by the following equation:

$$SNR = 10\log_{10}\frac{\sum_{n=1}^{N}(x(n) - \tilde{x}(n))^2}{\sum_{n=1}^{N}(x(n))^2} \quad (16)$$

It is important to note that an efficient denoising method would provide low MSE and PRD values as well as high SNR values.

3. RESULTS AND DISCUSSION

In this section, the effect of different parameters, such as various mother wavelets, different thresholding functions, different thresholding selection approaches, and different decomposition levels, is evaluated and discussed using the performance metrics mentioned in the previous section.

3.1. EVALUATION OF DIFFERENT MOTHER WAVELETS

A study was conducted in this section to determine which mother wavelet and order provide the best denoising performance. To compare their performance, MSE, NMSE, RMSE, NRMSE, PRD, and SNR were computed for each case. In Figure 8, the similarity of selected mother wavelets with the original FBG data is shown, while the metrics for DWT calculated using Daubechies, Symlets, Biorthogonal, and Coifiets mother wavelets are shown in Table (1). The thresholding was accomplished using a HT function and the rigsure thresholding approach. The results in Table (1) show that db9, sym7, bior5.5, and coif2 wavelets exhibit the highest performance in terms of low MSE, NMSE, RMSE, NRMSE, PRD and high SNR.

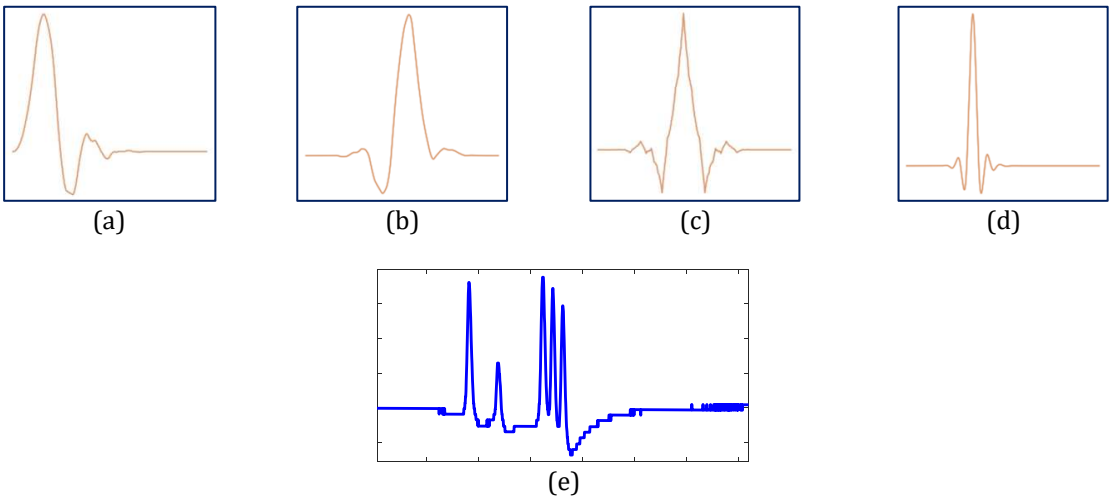

Figure 8 *Shape of : (a) Daubechies (b) Symlets (c) Biorthogonal (d) Coiflets (e) FBG strain signal for 5-axle truck*

Table (1) *Evaluation of denoising performance metrics for four different mother wavelets with multiple orders for sensor 2.*

		MSE	NMSE	RMSE	NRMSE	PRD	SNR
Noisy FBG signal		0.0454	0.0661	0.2131	0.2572	25.720	11.794
Mother wavelet	**Order**						
Daubechies wavelet	db6	0.0126	0.0184	0.1125	0.1357	13.574	17.345
	db7	0.0128	0.0186	0.1131	0.1365	13.653	17.295
	db8	0.0130	0.0190	0.1143	0.1379	13.790	17.208
	db9	**0.0124**	**0.0181**	**0.1116**	**0.1346**	**13.469**	**17.413**
	db10	0.0129	0.0188	0.1136	0.1371	13.713	17.257
Symlet wavelet	sym5	0.0127	0.0184	0.1127	0.1359	13.598	17.330
	sym6	0.0129	0.0187	0.1136	0.1371	13.711	17.258
	sym7	**0.0126**	**0.0184**	**0.1126**	**0.1350**	**13.590**	**17.334**
	sym8	0.0127	0.0184	0.1127	0.1359	13.599	17.329
	sym9	0.0128	0.0187	0.1133	0.1368	13.680	17.278
	sym10	0.0129	0.0188	0.1138	0.1373	13.732	17.245
	sym11	0.0127	0.0184	0.1127	0.1359	13.599	17.329
Biorthogonal wavelet	bior3.3	0.0151	0.0220	0.1229	0.1483	14.835	16.574
	bior3.5	0.0131	0.0191	0.1147	0.1384	13.841	17.176
	bior3.7	0.0131	0.0190	0.1144	0.1381	13.811	17.195
	bior3.9	0.0130	0.0189	0.1142	0.1378	13.780	17.214
	bior4.4	0.0127	0.0186	0.1130	0.1364	13.640	17.303
	bior5.5	**0.0127**	**0.0185**	**0.1128**	**0.1362**	**13.621**	**17.315**
	bior6.8	0.0128	0.0186	0.1131	0.1365	13.654	17.294
Coiflet wavelet	coif1	0.0133	0.0194	0.1155	0.1394	13.940	17.114
	coif2	**0.0124**	**0.0181**	**0.1117**	**0.1348**	**13.485**	**17.402**
	coif3	0.0128	0.0186	0.1132	0.1366	13.663	17.288

coif4	0.0127	0.0186	0.1130	0.1364	13.642	17.302
coif5	0.0128	0.0186	0.1131	0.1365	13.653	17.295

3.2. EVALUATION OF DIFFERENT THRESHOLDING FUNCTIONS

This study seeks to comprehend the influence of different thresholding functions and thresholding approaches on the denoising process. Figure 9 shows a raw noisy FBG signal and its denoised version using HT and ST approaches.

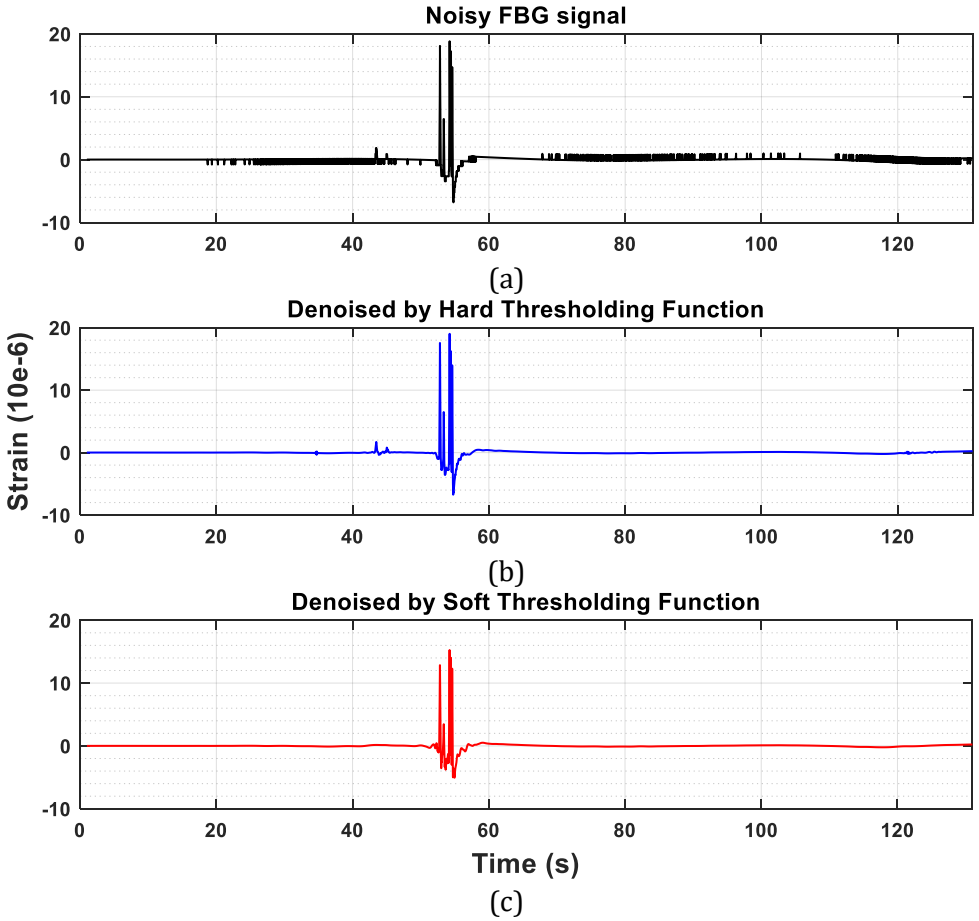

Figure 9 *FBG signals for sensor 2: (a) Raw noisy signal (b) Denoised signal using ST (c) Denoised signal using HT*

Figure 9 demonstrates that HT performed denoising better than ST, because ST remove the data by decreasing the amplitude. Next, the noisy FBG signals were decomposed using the db9, sym7, bior5.5, and coif2 mother wavelets from the previous evaluation. Then, the HT function was employed to ensure the conclusions. Finally, the effect of the thresholding approach, including sqtwolog, rigrsure, heursure, and minimaxi, was assessed. The metrics calculated for the HT function and various thresholding approaches are listed in Table (2).

Table (2) *Performance metrics for different thresholding approaches using four mother wavelets with a HT function for sensor 2.*

Mother wavelet and order	Threshold selection approach	MSE	NMSE	RMSE	NRMSE	PRD	SNR
Db9	sqtwolog	0.019	0.028	0.139	0.168	16.852	15.466
	rigrsure	**0.013**	**0.018**	**0.114**	**0.137**	**13.777**	**17.216**
	heursure	0.014	0.021	0.121	0.146	14.605	16.709
	minimax	0.033	0.048	0.183	0.221	22.114	13.106
Sym7	sqtwolog	0.019	0.027	0.137	0.166	16.642	15.575
	rigrsure	**0.012**	**0.018**	**0.113**	**0.136**	**13.667**	**17.286**
	heursure	0.014	0.020	0.119	0.143	14.391	16.837
	minimax	0.016	0.023	0.127	0.153	15.370	16.266
Bior5.5	sqtwolog	0.023	0.033	0.152	0.183	18.389	14.708
	rigrsure	**0.013**	**0.018**	**0.114**	**0.137**	**13.764**	**17.224**
	heursure	0.016	0.023	0.127	0.153	15.364	16.269
	minimax	0.016	0.024	0.129	0.156	15.632	16.119
coif2	sqtwolog	0.019	0.028	0.138	0.167	16.739	15.525
	rigrsure	**0.012**	**0.018**	**0.112**	**0.135**	**13.593**	**17.333**
	heursure	0.015	0.022	0.123	0.148	14.868	16.554
	minimax	0.016	0.023	0.127	0.154	15.404	16.247

From Table (2), it can be seen that the rigrsure threshold-based selection process provided the highest denoising performance in terms of low MSE, NMSE, RMSE, NRMSE, PRD and high SNR.

3.3. EVALUATION OF DIFFERENT DECOMPOSITION LEVELS

During the denoising process, the noisy FBG signals are decomposed using wavelet functions. The signal may still retain some noise if the DL is low whereas some vital signal information may be lost when the level is high. The number of decomposition levels and the appointed thresholding technique have a substantial effect on the SNR value. A study was carried out to find an optimal number of DLs for the wavelet functions and orders selected in the first evaluation. The rigrsure threshold selection approach was employed along with HT function. Figure 10 displays the SNR values calculated for various DLs ranging from level 1 to level 12. It is clear that the SNR value improved as the level of decomposition increased up to level 8; after that, SNR values remained relatively constant. Considering that a higher level of decomposition increases the calculation time, the optimal level of decomposition for denoising FBG signals was determined to be DL 8.

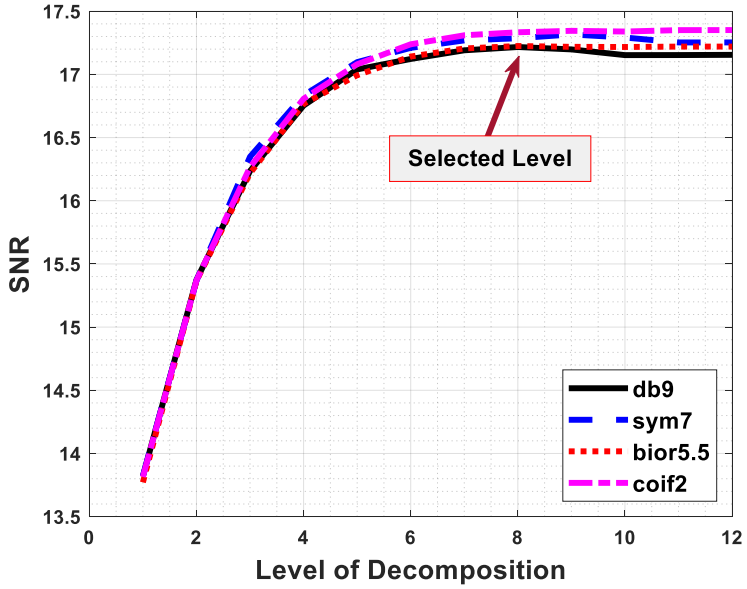

***Figure** 10 SNR values for various levels of decompositions (level 1-level 12): HT for sensor 2*

Denoising is mainly employed to enhance the SNR of signals and filter out noise components so that precision is improved. The SNR value is high when the settings indicated in Table (3) are used for FBG signal denoising, according to the previous evaluation.

***Table (3)** Selected optimal denoising parameters*

Mother Wavelet	Level of decomposition	Thresholding Function	Thresholding selection Approach
Db9 or sym7 or bior 5.5 or coif2	8	Hard thresholding	Rigrsure

Using the aforementioned parameters, a raw noisy FBG signal (130 s) was denoised and displayed in time domain as depicted in Figure 11 (a) and (b). Then, for better visualization, noisy and denoised signals were transferred from time domain to frequency domain and time-frequency domain as can be observed in Figure 11 (c)-(f). It is obvious that the FBG signal strongly improved and cleaned after the denoising process.

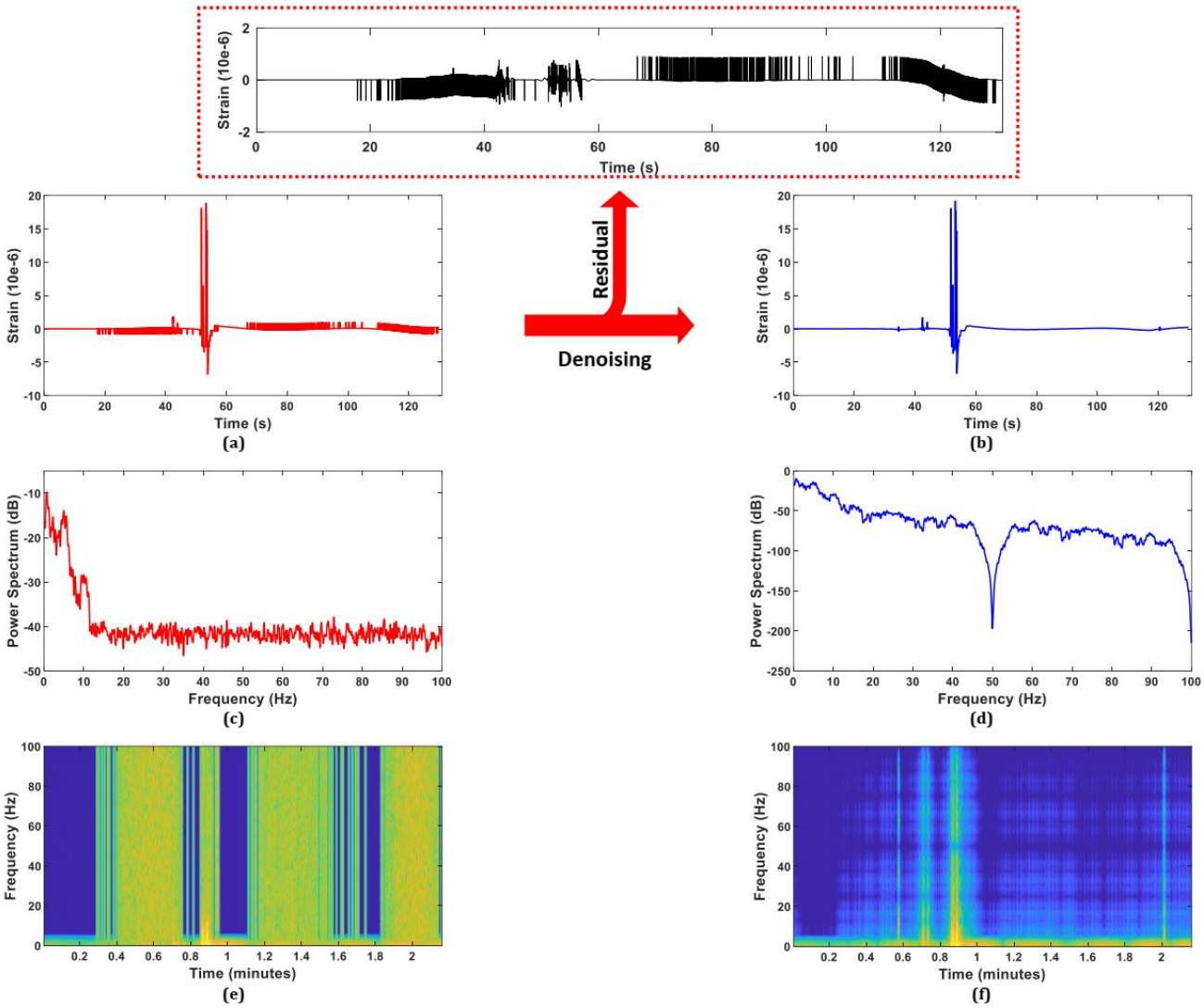

Figure 11 *Process of denoising the FBG signal: (a) Raw noisy signal in time domain (b) Denoised signal in time domain (c) Raw noisy signal infrequency domain (d) Denoised signal in time frequency domain (e) Raw noisy signal in time-frequency domain (f) Denoised signal in time-frequency domain*

3.4. COMPARISON STUDY

There are several methods for filtering and denoising in signal processing, each with its own strengths and weaknesses. For example, a low-pass filter is a type of filter that allows low-frequency components of a signal to pass through while attenuating high-frequency components. This filter is commonly used to remove high-frequency noise from a signal. A median filter is a nonlinear digital filter that is commonly employed for removing noise from a signal. It operates by replacing each data point in a signal with the median value of neighboring data points. A moving average filter is a linear filter that averages a certain number of neighboring samples in a signal. This filter is effective at smoothing out a signal and removing high-frequency noise.

In this section, these filters were compared for denoising the FBG sensor signal. The results in time and frequency domain are plotted in Figure 12. As it can be seen in Figure 12b, after denoising the signal using a low-pass filter, the power spectrum of the noise decreased dramatically in all ranges of frequency, but

the amount of noise that remained in the signal was considerable. Also, the amplitude of the data was reduced after denoising. By applying the median filter, there wass no remarkable change in either time domain or frequency domain. By utilizing a moving average filter, the power spectrum decreased in all ranges of frequency and especially at 40 and 80 Hz. This means that the power of noise decreased significantly, and the time domain shows that data amplitudes remained relatively unchanged. Finally, after denoising using the approach proposed in this study, the power spectrum of the signal decreased noticeably in all frequencies, especially at 50 Hz and 100 Hz. The time domain of the signal demonstrates that noise is removed from the signal without losing the amplitude of the data. The result of the evaluation of different filters listed in Table (4) and the results of performance evaluation validate the effectiveness of the proposed denoising approach based on DWT with optimum mother wavelet, level of decomposition, thresholding function, and thresholding selection approaches.

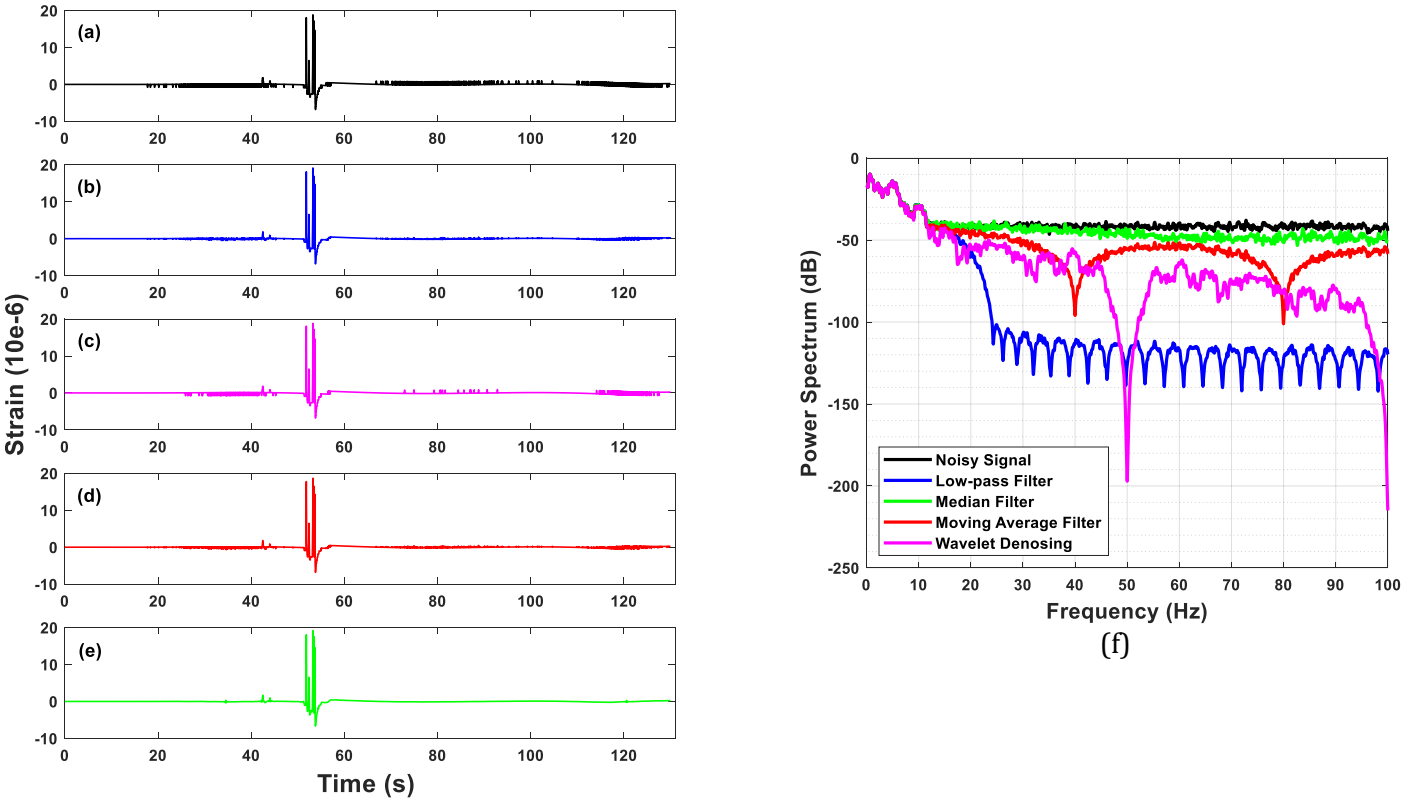

Figure 12 *FBG signals in time and frequency domain: (a) Raw noisy signal (b) Denoised signal using low-pass filter (c) Denoised signal using median filter (d) Denoised signal using moving average filter (e) Denoised signal using wavelet filter (f) FBG signals in frequency domain.*

Table (4) *Evaluation of the performance of different filter for denoising FBG signal*

Filtering Method	MSE	NMSE	RMSE	NRMSE	PRD	SNR
Low-Pass Filter	0.016	0.024	0.128	0.155	15.557	16.161

Median Filter	0.032	0.048	0.181	0.219	21.908	13.187
Moving Average Filter	0.017	0.025	0.133	0.160	16.087	15.870
Wavelet Denoising	**0.012**	**0.018**	**0.112**	**0.135**	**13.593**	**17.333**

4. CONCLUSIONS

The discretized wavelet transform (DWT) method was employed in this study to remove noise from FBG signals collected from pavement section and the following conclusions were drawn:

- Db9, sym7, bior 5.5, and coif2 were the mother wavelengths that exhibited the best performance.
- The hard thresholding function retained the amplitude of the FBG signal, but the soft thresholding function decreased the amplitudes dramatically and, for this reason, it is not a reasonable choice for denoising.
- The rigrsure thresholding approach provided the best results in terms of SNR, MSE, NMSE, RMSE, NRMSE, and PRD. Therefore, it can be the best approach for denoising FBG signals.
- The optimal level of decomposition was 8. Beyond this level, there was no further improvement in SNR.

Based on the findings from this study, it can be concluded that the presence of noise can significantly affect measurement precision, which emphasizes the importance of denoising techniques. Overall, this study provides valuable insights into the use of FBG sensors in SHM and highlights the importance of denoising techniques in ensuring accurate and reliable measurements.

Acknowledgments

This Ph.D. research (Characterization of asphalt pavement properties using fiber Bragg technology) is funded via Port of Antwerp-Bruges, Project 48231 “Durable Pavements for Port area - Heavily loaded pavements: exploration and in depth study”. Navid Hasheminejad would like to thank Research Foundation Flanders (FWO-Vlaanderen) for supporting with a postdoctoral fellowship (Postdoctoral Fellow - junior; 12ZU123N)

References

[1] X. Zhou, Research on Noise Removal in Fiber Grating Sensing Signal, International Journal of Advanced Network, Monitoring and Controls. 3 (2018) 87–91.

[2] D. Kong, J. Chang, P. Gong, Y. Liu, B. Sun, X. Liu, P. Wang, Z. Wang, W. Wang, Y. Zhang, Analysis and improvement of SNR in FBG sensing system, Photonic Sensors. 2 (2012) 148–157.

[3] P.X. ZHENG, Y.L. SONG, D.S. ZHANG, A. Wu, D.S. Jiang, Experimental study on temperature and strain sensing characteristics of fiber Bragg grating [J], Instrument Technology and Sensor. 22 (2008) 12–15.

[4] Z. Dong, X. Ma, X. Shao, Airport pavement responses obtained from wireless sensing network upon digital signal processing, International Journal of Pavement Engineering. 19 (2018) 381–390.

[5] D.L. Donoho, I.M. Johnstone, Ideal spatial adaptation by wavelet shrinkage, Biometrika. 81 (1994) 425–455.

[6] D. Gradolewski, G. Redlarski, Wavelet-based denoising method for real phonocardiography signal recorded by mobile devices in noisy environment, Comput Biol Med. 52 (2014) 119–129.

[7] S.R. Messer, J. Agzarian, D. Abbott, Optimal wavelet denoising for phonocardiograms, Microelectronics J. 32 (2001) 931–941.

[8] C. Torrence, G.P. Compo, A practical guide to wavelet analysis, Bull Am Meteorol Soc. 79 (1998) 61–78.

[9] S.K. Ghosh, R.N. Ponnalagu, Investigation of Discrete Wavelet Transform Domain Optimal Parametric Approach for Denoising of Phonocardiogram Signal, J Mech Med Biol. (2022).

[10] Y. Chen, L. Chen, H. Liu, K. Wang, Research on FBG sensor signal wavelength demodulation based on improved wavelet transform, Optik (Stuttg). 124 (2013) 4802–4804.

[11] Q. Zhang, B. Yu, S. Zhao, R. Tao, J. Peng, X. Wu, A novel method to reduce noise induced along transmission fiber for low-coherence interferometer, Optik (Stuttg). 124 (2013) 845–847.

[12] Y. Chen, Y. Cheng, H. Liu, Application of improved wavelet adaptive threshold de-noising algorithm in FBG demodulation, Optik (Stuttg). 132 (2017) 243–248.

[13] H. Jiang, D. Li, X. Zhang, Z. Ma, T. Lu, X. Shao, Research on de-noising method of fiber grating multiplexing network based on LCEEMD-LWT, Optik (Stuttg). 247 (2021) 167997.

[14] J. Su, Y. Qin, H. Zheng, W. Lu, S. Sun, Noise suppression for phase-sensitive optical time-domain reflectometer based on non-local means filtering, Optical Fiber Technology. 74 (2022) 103119.

[15] H. Wu, L. He, H. Chen, W. Xiao, Z. Guo, J. Duan, X. He, The improved denoising algorithm of acoustic sensor based on linear optical fiber Sagnac interferometer, Optical Fiber Technology. 60 (2020) 102363.

[16] Z. Lv, Y. Wu, W. Zhuang, X. Zhang, L. Zhu, A multi-peak detection algorithm for FBG based on WPD-HT, Optical Fiber Technology. 68 (2022) 102805.

[17] N. Li, J. Wang, B. Deng, F. Dong, An analysis of EEG when acupuncture with Wavelet entropy, in: 2008 30th Annual International Conference of the IEEE Engineering in Medicine and Biology Society, IEEE, 2008: pp. 1108–1111.

[18] P. Lall, D.R. Panchagade, P. Choudhary, S. Gupte, J.C. Suhling, Failure-envelope approach to modeling shock and vibration survivability of electronic and MEMS packaging, IEEE Transactions on Components and Packaging Technologies. 31 (2008) 104–113.

[19] C. He, J. Xing, J. Li, Q. Yang, R. Wang, A new wavelet threshold determination method considering interscale correlation in signal denoising, Math Probl Eng. 2015 (2015).

[20] M. Üstündağ, A. Şengür, M. Gökbulut, F. Ata, Performance comparison of wavelet thresholding techniques on weak ECG signal denoising, Przegląd Elektrotechniczny. 89 (2013) 63–66.

[21] N. Verma, A.K. Verma, Performance analysis of wavelet thresholding methods in denoising of audio signals of some Indian Musical Instruments, Int. J. Eng. Sci. Technol. 4 (2012) 2040–2045.

[22] S.K. Ghosh, R.K. Tripathy, R.N. Ponnalagu, Evaluation of performance metrics and denoising of PCG signal using Wavelet Based Decomposition, in: 2020 IEEE 17th India Council International Conference (INDICON), IEEE, 2020: pp. 1–6.